Structural and Electrochemical Characterization of Binary, Ternary, and Quaternary Platinum Alloy Catalysts for Methanol Electro-oxidation[1]

Bogdan Gurau, Rameshkrishnan Viswanathan, Renxuan Liu, Todd J. Lafrenz, Kevin L. Ley, and E. S. Smotkin*

Department of Chemical and Environmental Engineering, Illinois Institute of Technology, Chicago, Illinois 60616

Erik Reddington, Anthony Sapienza, Benny C. Chan, and Thomas E. Mallouk*

Department of Chemistry, The Pennsylania State University, University Park, Pennsylvania 16802

S. Sarangapani

ICET, Inc., Norwood, Massachusetts 02062

Received: July 7, 1998; In Final Form: October 6, 1998

The bifunctional model for methanol electro-oxidation suggests that competent catalysts should contain at least two types of surface elements: those that bind methanol and activate its C−H bonds and those that adsorb and activate water. Our previous work considered phase equilibria and relative Pt−C and M−O (M = Ru, Os) bond strengths in predicting improved activity among single-phase Pt−Ru−Os ternary alloys. By addition of a correlation with M−C bond strengths (M = Pt, Ir), it is possible to rationalize the recent combinatorial discovery of further improved Pt−Ru−Os−Ir quaternaries. X-ray diffraction experiments show that these quaternary catalysts are composed primarily of a nanocrystalline face-centered cubic (fcc) phase, in combination with an amorphous minor component. For catalysts of relatively high Ru content, the lattice parameter deviates positively from that of the corresponding arc-melted fcc alloy, suggesting that the nanocrystalline fcc phase is Pt-rich. Anode catalyst polarization curves in direct methanol fuel cells (DMFC's) at 60 °C show that the best Pt−Ru−Os−Ir compositions are markedly superior to Pt−Ru, despite the higher specific surface area of the latter. A remarkable difference between these catalysts is revealed by the methanol concentration dependence of the current density. Although the rate of oxidation is zero order in [CH_3OH] at potentials relevant to DMFC operation (250−325 mV vs RHE) at Pt−Ru, it is approximately first order at Pt−Ru−Os−Ir electrodes. This finding implies that the quaternary catalysts will be far superior to Pt−Ru in DMFC's constructed from electrolyte membranes that resist methanol crossover, in which higher concentrations of methanol can be used.

Introduction

One of the factors limiting the practical development of direct methanol fuel cells (DMFC's) is the poor performance of Pt alloy catalysts that perform the anode reaction 1:

$$CH_3OH + H_2O \rightarrow CO_2 + 6H^+ + 6e^- \quad (1)$$

Although the oxidation of methanol is rapid on clean Pt, CO appears as an intermediate in the reaction and poisons the surface.[2] The turnover of catalytic sites involves oxidation of CO to CO_2, using oxygen atoms supplied by water. Pt does not adsorb H_2O at potentials negative of about 0.4 V vs RHE. Pure Pt anodes are therefore relatively poor catalysts for reaction 1.

Alloys of Pt with more oxophilic elements have been investigated for many years as methanol electro-oxidation catalysts.[3] The superior performance of binary catalysts (Pt−Sn, Pt−Re, Pt−Mo, and Pt−Ru[4−8]) relative to Pt has been ascribed to two effects.[9,10] In the bifunctional model, the oxophilic metal is thought to provide sites for water adsorption. In the ligand-effect or electronic model, the role of the alloying element is to modify the electronic properties of Pt by contributing d-electron density. Beden et al. have proposed a detailed mechanism for the oxidation of methanol at Pt electrodes.[11] The sequence of reactions 2−5, in which M represents an alloying component or promoter metal, is based on their mechanism as modified for alloys by Freelink and co-workers:[12]

$$Pt + CH_3OH \rightarrow Pt-(CH_3OH)_{ads} \quad (2)$$

$$Pt-(CH_3OH)_{ads} \rightarrow Pt-(CH_3O)_{ads} + H^+ + e^- \quad (3a)$$

$$Pt-(CH_3O)_{ads} \rightarrow Pt-(CH_2O)_{ads} + H^+ + e^- \quad (3b)$$

$$Pt-(CH_2O)_{ads} \rightarrow Pt-(CHO)_{ads} + H^+ + e^- \quad (3c)$$

$$Pt-(CHO)_{ads} \rightarrow Pt-(CO)_{ads} + H^+ + e^- \quad (3d)$$

$$M + H_2O \rightarrow M-(H_2)_{ads} \quad (4)$$

$$Pt-(CO)_{ads} + M-(H_2O)_{ads} \rightarrow Pt + M + CO_2 + 2H^+ + 2e^- \quad (5)$$

The best choice of alloying element(s) for an anode electrocatalyst depends on which step in this reaction sequence is rate-limiting. Oxophilic additives will directly affect the rates of

10.1021/jp982887f CCC: $15.00
Published on Web 12/03/1998

reactions 4 and 5 and, indirectly through electronic effects,[13−15] the rates of reactions 2 and 3.[16,17] Most studies in this area have considered reactions 4 and 5 as the rate-determining steps under different conditions and have focused, for reasons of simplicity, on binary Pt alloys. Recently, we investigated the simultaneous addition of two oxophilic alloying elements (Ru and Os) to Pt. Os is more oxophilic than Ru but significantly less soluble in face-centered cubic (fcc) Pt. The best catalytic performance was therefore found at ternary compositions near the Os solubility limit.[18] To explore more complex compositions, we subsequently developed a rapid combinatorial screening method for ternary and quaternary alloy catalysts.[19] The surprising result of this later study was that the addition of small amounts of Ir to the Pt−Ru−Os ternary catalysts significantly improved their performance. Interestingly, with the exception of Pt−Ru−Os, the ternary compositions bounding this quaternary region of phase space (Pt−Ru−Ir and Pt−Os−Ir) are relatively poor catalysts.

In this paper, we examine these results in light of phase equilibria and M−C and M−O bond strengths. The composition of the best quaternary catalysts is again in accord with estimates of the maximum solubility of the alloying elements in fcc Pt. The role of Ir appears to be different from that of Ru and Os, since Ir forms relatively strong bonds to C but not to O. Remarkably, unlike Pt−Ru, these complex alloy catalysts show an approximately first-order rate dependence in [CH_3OH] under conditions relevant to the operation of DMFC's. This result implies that earlier steps in the reaction mechanism, which involve C−H bond activation, are rate-determining for the Pt−Ru−Os and Pt−Ru−Os−Ir alloys and that the role of Ir is to accelerate these processes.

Experimental Section

Preparation of Arc-Melted Alloys. Pt and Pt alloy samples were prepared by arc-melting pressed pellets of Pt, Ru, Os, and Ir powders (Johnson Matthey) under Ar. The precursor metal powders were intimately mixed in the appropriate proportions.[20] After six melt cycles, the alloy ingots were machined and polished to make flat, mirror-finish samples for X-ray diffraction (XRD) and electrochemical analysis.

Preparation of Unsupported High Surface Area Catalysts. High surface area catalysts containing Pt, Ru, Os, and Ir were prepared by reduction of aqueous solutions of H_2PtCl_6 and the respective metal chloride salts in the desired stoichiometry using $NaBH_4$ (Aldrich). The reduction of metal ions in these solutions was essentially quantitative under the conditions used. All catalyst precursor salt solutions were in the range 2−10 mM in total metal content and were analyzed by ICP-AES.

X-ray Photoelectron Spectroscopy (XPS) and X-ray Diffraction. X-ray photoelectron spectra (XPS) were obtained with a Kratos XSAM 800 PCI spectrometer, which had a Mg Kα line source. Powder samples were mounted on carbon tape, and spectra were obtained with a 40 eV pass energy, and at a 15° take-off angle from the surface normal. Binding energies were referenced to a graphite standard (C 1s = 284.5 eV). Survey spectra were performed at a resolution of 1 eV, and quantitative surface compositions were measured by integration of slower scans taken at a resolution of 0.1 eV. Apparent atomic percentages were obtained by dividing integrated peak areas by atomic sensitivity factors.

X-ray diffraction patterns were recorded on a General Electric XRD5 diffractometer and on a Philips X'Pert MPD diffractometer, using monochromatized Cu Kα radiation. Accurate lattice parameters were obtained on the XRD5 using an external silicon standard and a profile fitting routine that compensated for sample displacement errors and other instrumental parameters, such as beam divergence and absorption. Data were obtained on the Philips instrument with an internal standard (Cu or Al) and were corrected for measurement error by determining the cubic lattice parameter from each peak and then extrapolating the results to $2\theta = 180°$. Derived lattice constants from the two instruments were in agreement to an accuracy of ±0.002 Å.

Surface Area Measurements. Surface area measurements for all catalysts were carried out on a Micromeritics ASAP 2010 instrument. Standard isotherms were obtained using N_2 at 77 K, and a multipoint BET analysis with the adsorption data from $0.08 < P/P_0 < 0.15$ was used for surface area calculations. All samples were dried under vacuum at 110 °C for 3 h prior to analysis. The catalysts all exhibited type 3 isotherms, with no apparent hysteresis loop in the desorption curve. This behavior indicates that the adsorbent (catalyst) and adsorbate (N_2) interactions are very weak and that no capillary condensation is occurring in the larger pores of the materials.

Liquid-Feed DMFC Studies. DMFC performance curves were obtained using unsupported anode catalysts and Pt black (Johnson-Matthey) as the cathode. All anode and cathode catalyst loadings were approximately 4 mg/cm^2. The membrane electrode assemblies (MEA's) were prepared by decal transfer of catalyst inks (10 wt % soluble Nafion relative to dry catalyst) onto Nafion 117 membranes.[21] Methanol−water solution was delivered to the 5 cm^2 anode at 12.5 mL/min (0 psig back pressure), while dry air (0 psig, 400 mL/min) was delivered to the cathode. The cell was maintained at 60 °C, and the MEA's were conditioned by holding the cell at a voltage of 200 mV for 3 days prior to acquiring $i-V$ data. Fuel cell $i-V$ curves were measured using a Scribner Associates series 890 fuel cell load. The polarization curves were IR-compensated and were measured vs a reversible hydrogen electrode (RHE). The RHE consisted of a small spot of unsupported Pt on the Nafion membrane, approximately 0.5 cm from the edge of the anode catalyst. A Pt electrode affixed to the end of a Teflon plug, which was press-fitted into a hole drilled through the carbon block, made contact with the reference. The flow rate of zero-grade hydrogen into the reference port was 1 mL/min. Leakage of hydrogen from the RHE into the anode is prevented by means an O-ring.

Results and Discussion

Figure 1 shows a plot of the gas-phase bond dissociation energies of M−C and M−O diatomic compounds.[22] The most oxophilic elements are earlier transition metals (Ti, V, W, Re, Os) and post-transition elements (Ge, Sn). For M−C compounds, the maximum in bond strength appears at Ru in the second transition series and at Ir in the third. Although these bond strengths, derived from gas-phase diatomics, can only provide a rough guideline for electrochemical processes occurring at the metal/solution interface, some interesting trends emerge. The strength of the Pt−O bond is considerably less than that of the other M−O compounds of catalytic interest, i.e., Ru, Os, Re, Mo, Sn. Combining Pt with these oxophilic elements gives a more active anode catalyst. Note that Os appears to be more oxophilic than Ru in the plot, consistent with the relative ease of electrochemical oxidation of the two metals. Os is known to adsorb water in acidic solutions at potentials slightly more negative than does Ru.[23] The Ir−O bond is relatively weak and similar in strength to Pt−O, but the Ir−C bond is quite strong and close in strength to Pt−C. This is an

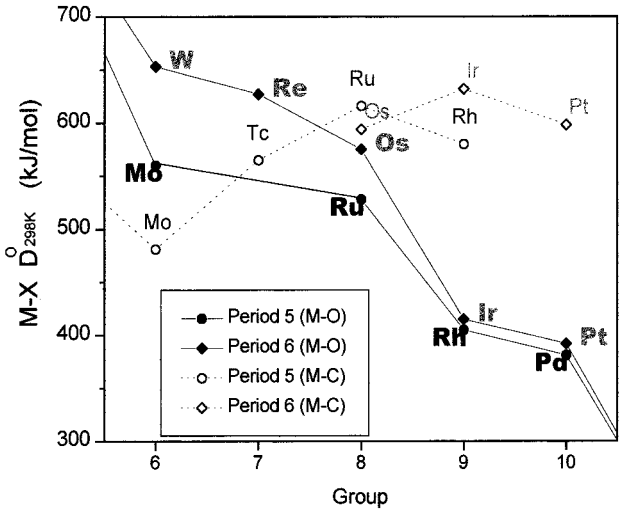

Figure 1. M−O and M−C bond strengths for gas-phase diatomic compounds.

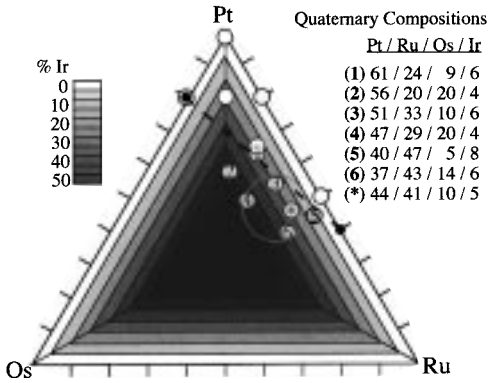

Figure 2. Pt−Ru−Os−Ir composition map, looking through the Pt−Ru−Os ternary face. Increasing Ir concentration is shown in gray scale. Black dots on the Pt−Ru and Pt−Os axes show the binary solubility limits, and the single-phase ternary region is approximately defined by the area above the dashed line joining these binary limits. Anode catalyst compositions are indicated by open circles, and the region of highest catalytic activity is shown as a circle containing the best catalyst found by combinatorial screening, $Pt_{44}Ru_{41}Os_{10}Ir_5$ (*).

indication that the improved performance of the Pt−Ru−Os−Ir quaternary catalyst, relative to Pt−Ru−Os, is not a sole consequence of accelerating reaction 4. Rather, it suggests that the improvement is in the ability of Ir to make bonds to C, as required in step 3.

A related issue is why the best catalysts found by combinatorial search methods[15] contain relatively small amounts of the elements Os (10 atom %) and Ir (5%). These elements make stronger M−O and M−C bonds, respectively, than the major components of the catalyst, Pt and Ru. Figure 2 shows a view of the quaternary composition space considered in this study. The figure shows the Pt−Ru−Os face of the tetrahedral composition diagram, with the gray scale indicating depth along the Ir axis. One can approximate the single-phase Pt−Ru−Os ternary region of the diagram by drawing a line between the points of maximum solubility of Ru and Os in fcc Pt.[24,25] The solubility of Ir is quite low (about 6%) in the fcc Pt phase below 600 °C. By considering these approximate solubility limits, it appears that the best catalysts are those that maximize the content of Ru, Os, and Ir *in the fcc Pt phase*. Higher concentrations of Os or Ir in fcc Pt would lead to the formation of other phases, which are not likely to be good catalysts.

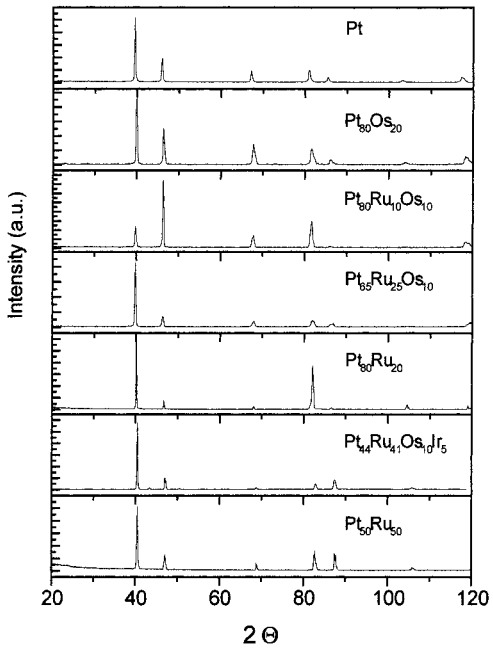

Figure 3. X-ray diffraction patterns of arc-melted Pt alloys. Small peaks in the $Pt_{44}Ru_{41}Os_{10}Ir_5$ pattern are from a Cu internal standard. Subscripts indicate atomic percentages.

The issue of phase stability was studied by preparing representative binary, ternary, and quaternary compositions in two forms. One form was an arc-melted alloy prepared from the appropriate mixture of pure metals. The other form was a high surface area catalyst, made by rapid borohydride reduction of aqueous metal salts. Figure 3 shows X-ray diffraction patterns of arc-melted alloys varying in composition from 100% to 44% Pt. All of these patterns show a single fcc phase, and no detectable amount (i.e., <1−2%) of any other crystalline phases, such as hexagonal close-packed (hcp) Os, Ru, or Ru−Os. The fact that the $Pt_{44}Ru_{41}Os_{10}Ir_5$ composition is single-phase fcc indicates that the linear interpolation in Figure 2 slightly underestimates the solubility limits of the alloying elements. Therefore, most or all of the compositions considered here should be thermodynamically stable as single-phase fcc alloys, at least in bulk form.

The powder XRD pattern of a representative high surface area catalyst, $Pt_{51}Ru_{33}Os_{10}Ir_6$, is shown in Figure 4. As prepared, the pattern shows only a nanocrystalline fcc phase. The primary particle size, as determined from the line widths by means of the Scherrer equation,[26] is on the order of 9−10 nm. The $Pt_{51}Ru_{33}Os_{10}Ir_6$ sample, which is representative of high surface area catalysts with Pt content less than about 65%, was heated to progressively higher temperatures under Ar, and XRD patterns were then recorded at ambient temperature. Below about 300 °C there is no change in the pattern. However, in the sample heated to 500 °C, a poorly ordered or nanocrystalline hcp phase appears as a minor component, as evidenced by the broad diffraction peak at 43.6° 2θ. In the sample heated to 700 °C, diffraction lines attributed to both the cubic and hexagonal phases become sharper, indicating that the primary particles are sintering into larger aggregates. After heating to 1000 °C, there appear to be two fcc phases with slightly different lattice parameters and the intensity of diffraction peaks from the hcp phase is substantially decreased.

The appearance at intermediate temperatures of the hcp phase, which is most likely Ru or Ru−Os, suggests two possibilities. One is that the catalyst, as prepared, contains a single nanocrystalline phase, which disproportionates upon heating to a Pt-

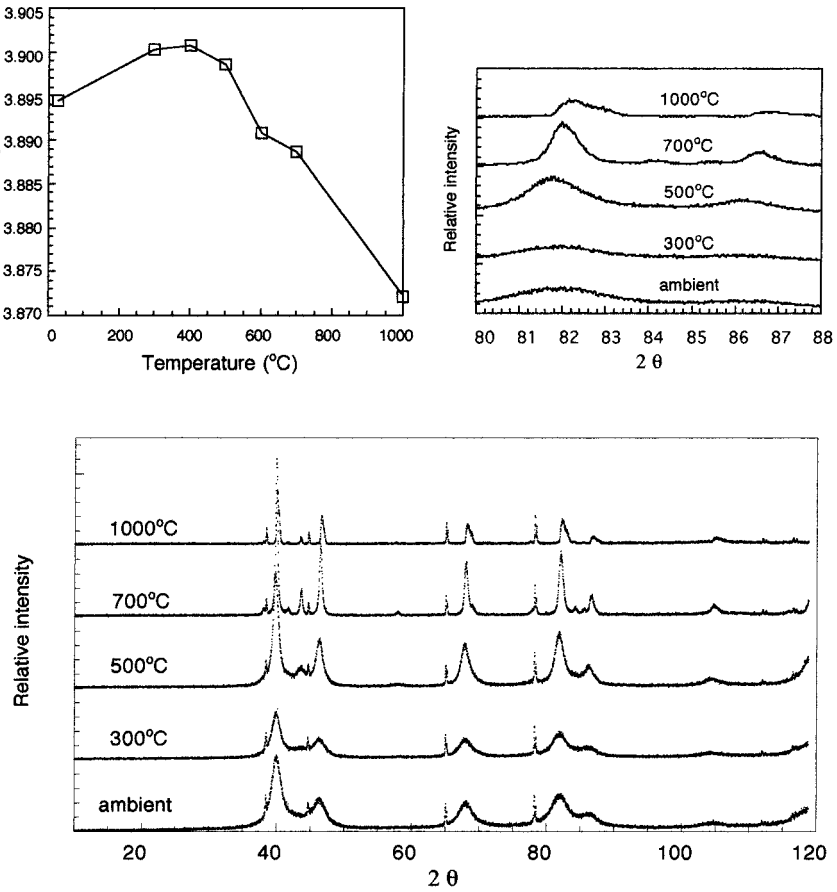

Figure 4. X-ray powder diffraction patterns (measured at room temperature) of $Pt_{51}Ru_{33}Os_{10}Ir_6$, from bottom, as prepared, and heated progressively to 300, 500, 700, and 1000 °C under Ar. Small sharp lines to the left of each fcc peak are from the Al internal standard. Inset at upper right shows an expanded view of the (311) and (222) reflections of the fcc phase. Inset at upper left shows changes in the fcc lattice constant.

TABLE 1: BET Surface Areas of Pt−Ru−Os−Ir Catalysts (Borohydride Reduction Method)

catalyst composition	surface area (m^2/g)
$Pt_{50}Ru_{50}$	25
$Pt_{61}Ru_{24}Os_9Ir_6$	29
$Pt_{56}Ru_{20}Os_{20}Ir_4$	19
$Pt_{51}Ru_{33}Os_{10}Ir_6$	27
$Pt_{47}Ru_{29}Os_{20}Ir_4$	38
$Pt_{40}Ru_{47}Os_5Ir_8$	26
$Pt_{37}Ru_{43}Os_{14}Ir_6$	39

rich fcc phase and a Ru-rich hcp phase. The second is that the Ru-rich component is initially present in amorphous form, either in the zerovalent state or as a hydrous oxide, and that the hcp phase forms from this amorphous component. In either case, heating to high temperatures generates the thermodynamically stable fcc alloy. This issue can be resolved by examining the insets in Figure 4. They show an expanded view of the XRD patterns in the vicinity of the (311) reflection and calculated changes in the lattice parameters with heating, as determined from all the reflections in the pattern. Progressive heating of the samples causes the lattice parameter of the fcc phase first to increase slightly and then to decrease significantly with the disappearance of the hcp phase. The initial increase could be interpreted as loss of a small amount of Ru from the high surface area fcc phase. However, the increase is small compared to the final decrease, suggesting that most of the hcp phase arises from an amorphous component in the as-prepared sample.

This interpretation is also supported by a comparison of the lattice parameters of the arc-melted alloys and the as-prepared catalysts, as shown in Figure 5. The lattice parameters for the Pt−Ru alloys have been reported previously[18] and are in good

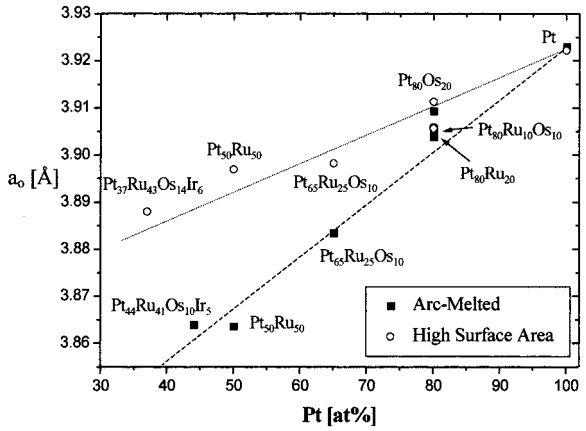

Figure 5. Comparison of lattice parameters of the fcc phase for high surface area catalysts and arc-melted alloys.

agreement with the available literature values.[27] For the arc-melted alloys, the lattice parameter decreases smoothly with decreasing Pt content, consistent with the smaller size of the Ru atom and the higher average bond strength in the alloys, relative to pure Pt. At high atomic percentages of Pt, the lattice parameters of the high surface area catalysts and the single-phase alloys are nearly coincident. However, at 65% Pt and below, the lattice parameter of the fcc phase in the catalysts is between those of Pt and the corresponding arc-melted alloy. Although these results should be interpreted cautiously, because of the high proportion of surface atoms, the trend does support the idea that the nanocrystalline fcc phase is enriched in Pt relative to the overall composition of the catalyst.

TABLE 2: XPS Binding Energies and Apparent Surface Compositions of High Surface Area Pt−Ru−Os−Ir Catalysts

	apparent atomic percentages (binding energies, eV)				
catalyst	Pt 4f	O 1s	Ru 3d	Ir 4f	Os 4f
$Pt_{47}Ru_{29}Os_{20}Ir_4$	8.8 (71.4)	60.7 (531.0)	18.6 (280.6)	4.2 (61.4)	7.7 (51.0)
$Pt_{40}Ru_{47}Os_5Ir_8$	6.0 (71.4)	64.7 (531.0)	15.7 (280.5)	12.1 (61.2)	1.5 (50.8)
$Pt_{37}Ru_{43}Os_{14}Ir_6$	6.8 (71.4)	64.4 (530.8)	18.8 (280.6)	5.3 (61.4)	4.7 (50.9)

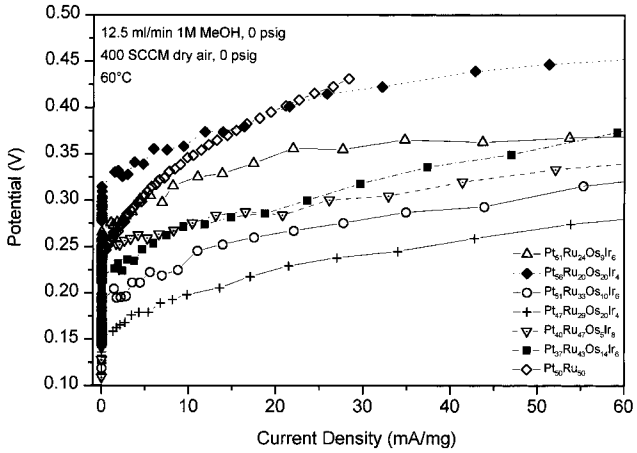

Figure 6. DMFC anode polarization curves for Pt−Ru−Os−Ir quaternary catalysts. Geometrical electrode areas were 5 cm^2, with catalyst loadings of ca. 4 mg/cm^2. Potentials are referenced to RHE, and the current is mass-normalized. Anode conditions are the following: 12.5 mL/min, 1.0 M methanol, 0 psig, 60 °C. Cathode conditions are the following: 400 sccm dry air, 0 psig. The electrolyte is Nafion 117.

Surface atomic compositions derived from XPS spectra (Table 2) also support the idea that the high surface area catalysts, as prepared, contain surface phases that are enriched in Ru, Os, and Ir. The most striking feature of these spectra is the high oxygen content of the surface, which is consistent with the presence of an oxide or hydrated oxide phase. The low apparent Pt content indicates that the surface phases are 1−2 nm thick oxide films. The Pt binding energy is in the range expected for metallic Pt, and not for Pt oxides, which are typically about 2 eV higher.[28] The binding energy of Ru is in the range expected for RuO_2 (280.5−281.0 eV) rather than Ru metal (279.8−280.2 eV). The Os and Ir binding energies are also higher than those expected for metals (50.2−50.6 and 60.5−61.0 eV, respectively), consistent with the presence of a mixed metal oxide.

As noted in the Introduction, the addition of oxophilic alloying elements or adatoms enhances the activity of Pt-based anode catalysts. However, it is important to balance the oxophilic character of an added element with its tendency to be oxidized in the DMFC. For example, the activity of Sn-containing catalysts is believed to derive, at least in part, from the presence of oxidized Sn ions in solution.[10,29] Although a mixed metal oxide appears to cover the bulk phases of Pt−Ru−Os−Ir catalysts, as prepared, it is important to note that this structure is unlikely to persist under conditions of fuel cell operation.

Electrochemical XPS studies of the single phase arc-melted analogues of the high surface area catalysts indicate a potential-dependent distribution of oxides.[30] There is good evidence that Ru adatoms on Pt are reduced to the zerovalent state in the potential range of interest (0.2−0.5 V vs RHE). Binary Pt−Ru (1:1) alloy surfaces are known to be resistant to Pt-enrichment, caused by preferential Ru dissolution, up to ca. 1.0 V.[31] The arc-melted Os-containing alloys used in this work were stable up to 0.8 V in 0.5 M H_2SO_4.[18] Prolonged potential cycling of these electrodes at 100 mV/s to an upper limit of 0.8 V produced no voltammetric features in the hydrogen region characteristic of Pt enrichment. However, when the upper limit was increased to 1.2 V, distinctive H adsorption/desorption

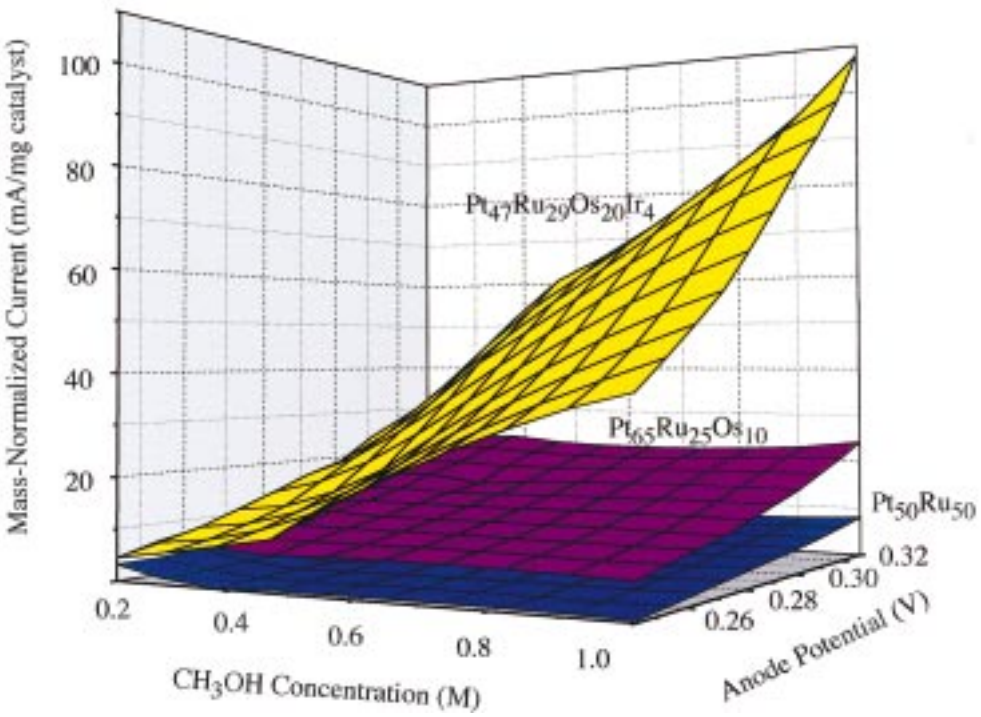

Figure 7. Mass-normalized current vs methanol concentration and anode potential for high surface area $Pt_{50}Ru_{50}$, $Pt_{65}Ru_{25}Os_{10}$, and $Pt_{47}Ru_{29}Os_{20}Ir_4$ catalysts.

waves, double-layer features, and metal oxide reduction peak values characteristic of Pt emerged. A more complete study of the surface oxidation states of these catalysts in operating fuel cells is currently in progress and will be described in a separate publication.[30]

Figure 6 shows anode polarization curves from six quaternary catalysts, compared with $Pt_{50}Ru_{50}$, in a DMFC fitted with a hydrogen reference electrode. The performance of $Pt_{47}Ru_{29}Os_{20}Ir_4$ and quaternaries of similar composition, relative to $Pt_{50}Ru_{50}$, is striking. The open-circuit voltage obtained with $Pt_{47}Ru_{29}Os_{20}Ir_4$ is 120 mV more positive than that of $Pt_{50}Ru_{50}$, and the current density of the quaternary is substantially higher at all potentials. By referring to the composition map (Figure 2), one can see that the three compositions ($Pt_{51}Ru_{33}Os_{10}Ir_6$, $Pt_{47}Ru_{29}Os_{20}Ir_4$, and $Pt_{37}Ru_{43}Os_{14}Ir_6$) that give the highest open-circuit voltages are located in a small region, which also contains the best combinatorially selected value ($Pt_{44}Ru_{41}Os_{10}Ir_5$). This zone of high activity is also roughly coincident with the fcc phase boundary.

Further insight into the higher activity of the quaternary catalysts can be obtained by measuring the concentration dependence of the current, using the same membrane electrode assembly. Figure 7 shows a three-dimensional plot of mass-normalized current in the DMFC vs methanol concentration and anode potential for $Pt_{47}Ru_{29}Os_{20}Ir_4$, $Pt_{65}Ru_{25}Os_{10}$, and $Pt_{50}Ru_{50}$. Anode polarization curves were measured at 0.250, 0.375, 0.500, and 1.00 M methanol. The lower part of the figure shows data obtained with $Pt_{50}Ru_{50}$ and is consistent with previous observations that Pt−Ru/C and Pt−Ru catalysts follow zero-order kinetics with respect to methanol concentration at low potentials.[32] For $Pt_{50}Ru_{50}$ at low potentials, the rate-determining step involves the activation of water (reaction 4). At higher potentials (>400 mV), where the activation of water is facile, the current density becomes first order in methanol concentration, as expected from the mechanisms of Beden et al.[11] and Freeling et al.[12]

Remarkably, the current at the quaternary catalyst shows an approximately first-order dependence on methanol concentration, even at potentials as low as 250 mV. Apparently, the high Os content of this catalyst is sufficient to render reaction 4 rapid, relative to reaction 3, over the entire range of conditions represented in Figure 7. At the highest methanol concentration used, 1.00 M, the anode performance of $Pt_{47}Ru_{29}Os_{20}Ir_4$ is *several times higher* than that of $Pt_{50}Ru_{50}$. Despite this first-order rate dependence, the overall performance of DMFC's made from this quaternary catalyst, while markedly superior to those made from $Pt_{50}Ru_{50}$, is fairly insensitive to methanol concentration. The reason is that the performance of the *cathode* drops substantially at higher concentration because of the increasing methanol crossover rate. We note finally that improvements in polymer electrolyte membranes, with reduced crossover rates, should have a dramatic effect on the overall performance of DMFC's made from quaternary alloy anode electrocatalysts.

Conclusions

The picture that emerges from this study is that the best Pt−Ru−Os−Ir binary catalysts lie in a region of phase space that is close to the solubility limit of the three alloying elements in fcc Pt. The improved performance of these catalysts can be rationalized within a conceptual framework previously developed for Pt−Ru−Os ternary catalysts, which correlated M−O bond strength and phase stability with performance.[18] The ternary catalysts fit the bifunctional model for methanol oxidation, and the primary role of the alloying elements is to lower the potential for adsorption and activation of water. The addition of Ir appears to accelerate the activation of the C−H bonds in methanol, and indeed, this behavior is consistent with the substantial literature on C−H activation in Ir and Rh compounds.[33−35] The fact that the best alloying element for this purpose makes strong M−C (and M−H) bonds again suggests that other interesting compositions might be discovered by rational consideration of bond strengths, electrochemical stability, and phase equilibria, in combination with rapid and exhaustive combinatorial searches. Experiments along these lines are currently in progress.

Acknowledgment. We thank Vince Bojan for acquiring the XPS spectra. This work was supported by the U.S. Army Research Office and DARPA under Grants DAAH04-94-G-0055, DAAH04-95-1-0330, and DAAH04-95-1-0570.

References and Notes

(1) The authors join the other contributors to this issue in wishing Prof. Allen Bard a very happy birthday.

(2) Parsons, R.; VanderNoot, T. *J. Electroanal. Chem.*. **1988**, *257*, 9.

(3) Koch, D. F. A. Australian Patent 46123, 1964.

(4) Rauhe, B. R., Jr.; McLarnon, F. R.; Cairns, E. J. *J. Electrochem. Soc.* **1995**, *142*, 1073.

(5) Bockris, J. O'M.; Wroblowa, H. *J. Electroanal. Chem.* **1964**, *7*, 428.

(6) Ross, P. N. In *Proceedings of the Workshop on Direct Methanol−Air Fuel Cells*; Landgrebe, A. R., Sen, R. K., Eds.; The Electrochemical Society: Pennington, NJ, 1992; Vol. 92-14, p 51.

(7) Freelink, T.; Visscher, W.; van Veen, J. A. R. *Electrochim. Acta* **1994**, *39*, 1871.

(8) Freelink, T.; Visscher, W.; Cox, A. P.; van Veen, J. A. R. *Electrochim. Acta* **1995**, *40*, 1537.

(9) Haner, A. N.; Ross, P. N. *J. Phys. Chem.* **1991**, *95*, 3740.

(10) Bae, I. T.; Takeshi, S.; Scherson, D. A. *J. Electroanal. Chem.* **1991**, *297*, 185.

(11) Beden, B.; Leger, J.-M.; Lamy, C. In *Modern Aspects of Electrochemistry*; Bockris, J. O'M, Conway, B. E., White, R. E., Eds.; Plenum Press: New York, 1992; Vol. 22, pp 97−247.

(12) Freelink, T.; Visscher, W.; van Veen, J. A. R. *Surf. Sci.* **1995**, *335*, 353.

(13) McBreen, J.; Mukerjee, S. *J. Electrochem. Soc.* **1995,** *142*, 3399.

(14) Iwasita, T.; Nart, F. C.; Vielstich, W. *Ber. Bunsen-Ges. Phys. Chem.* **1990**, *94*, 1030.

(15) Anderson, A. B.; Grantscharova, E.; Seong, S. *J. Electrochem. Soc.* **1996**, *143*, 2075.

(16) Sobkowski, J.; Franaszczak, K.; Piasecki, A. *J. Electroanal. Chem.* **1985**, *196*, 145.

(17) Il'chenko, N. I.; Golodets, G. I. *J. Catal.* **1975,** *39*, 73.

(18) (a) Ley, K. L.; Liu, R.; Pu, C.; Fan, Q.; Leyarovska, N.; Segre, C.; Smotkin, E. S. *J. Electrochem. Soc.* **1997,** *144*, 1543. (b) Liu, L.; Viswanathan, R.; Liu, R.; Smotkin, E. S. *Electrochem. Solid State Lett.* **1998**, *1*, 123.

(19) Reddington, E.; Sapienza, A.; Gurau, B.; Viswanathan, R.; Sarangapani, S.; Smotkin, E. S.; Mallouk, T. E. *Science* **1998**, *280*, 1735.

(20) Osmium is a toxic element, and care should be exercised in handling it. Poisoning occurs via the inhalation of OsO_4. However, Os metal, when alloyed or used under reducing conditions, is far less toxic. It is used in instrument pivots, electrical contacts, and fountain-pen tips.

(21) Wilson, M. S.; Gottesfeld, S. *J. Appl. Electrochem.* **1992**, *22*, 1.

(22) *CRC Handbook of Chemistry and Physics*, 77th ed.; Lide, D. R., Ed.; CRC Press: Boca Raton, FL, 1996.

(23) Appleby, A. J. *Surf. Sci.* **1971**, *27*, 225.

(24) (a) Hutchinson, J. M. *Platinum Met. Rev.* **1972**, *16* (3), 88. (b) *Binary Alloy Phase Diagrams*, 2nd ed.; Massalski, T., Ed.; ASM International: Materials Park, OH, 1990.

(25) Savitskii, E. M., Prince, A., Eds. *Handbook of Precious Metals*; Hemisphere Publishing Corp.: New York, 1989; p 231.

(26) Klug, H. P.; Alexander, L. E. *X-Ray Diffraction Procedures for Polycrystalline and Amorphous Materials*, 2nd. ed.; Wiley-Interscience: New York, 1974; pp 656−657.

(27) Gasteiger, H. A.; Markovic, N.; Ross, P. N., Jr.; Cairns, E. J. *J. Phys. Chem.* **1993**, *97*, 12020.

(28) Moulder, J. F.; et al. *Handbook of Photoelectron Spectroscopy, A Reference Book of Standard Spectra for the Identification and Interpretation of XPS Data*; Chastain, J., Ed.; Perkin-Elmer Corp.: Eden Prarie, MN, 1992; pp 150−181.

(29) Sobkowski, J.; Franaszczak, K.; Piasecki, A. *J. Electroanal. Chem.* **1985**, *196*, 145.

(30) Sung, Y.-E.; Thomas, S.; Wieckowski, A.; Liu, R.; Smotkin, E. S. Manuscript in preparation.

(31) Ticanelli, E.; Beery, J. G.; Paffet, M. T.; Gottesfeld, S. *J. Electroanal. Chem*. **1989**, *258*, 61.

(32) Liu, L.; Pu, C.; Viswanathan, R.; Fan, Q.; Liu, R.; Smotkin, E. S. *Electrochim. Acta* **1998**, *43*, 3657.

(33) Shilov, A. E. *Activation of Saturated Hydrocarbons by Transition Metal Complexes*; Dordrecht: Boston, 1984.

(34) (a) Jones, W. D.; Feher, F. J. *J. Am. Chem. Soc.* **1984**, *106*, 1650. (b) Jones, W. D.; Feher, F. J. *Acc. Chem. Res.* **1989**, *22*, 91. (c) Chin, R. M.; Dong, L.; Duckett, S. B.; Partridge, M. G.; Jones, W. D.; Perutz, R. D. *J. Am. Chem. Soc.* **1993**, *115*, 7685.

(35) Bengali, A. A.; Arndsten, B. A.; Burger, P. M.; Schultz, R. H.; Weiller, B. H.; Kyle, K. R.; Moore, C. B.; Bergman, R. G. *Pure Appl. Chem.* **1995**, *67*, 281.